Physics of the Earth and Planetary Interiors 215 (2012) 12–20

Contents lists available at SciVerse ScienceDirect

Physics of the Earth and Planetary Interiors

journal homepage: www.elsevier.com/locate/pepi

A comparison of ice VII formed in the H_2O, $NaCl–H_2O$, and $CH_3OH–H_2O$ systems: Implications for H_2O-rich planets

Mark R. Frank [a,*], Elizabeth Aarestad [a], Henry P. Scott [b], Vitali B. Prakapenka [c]

[a] Department of Geology and Environmental Geosciences, Northern Illinois University, DeKalb, IL 60115, United States
[b] Department of Physics and Astronomy, Indiana University South Bend, South Bend, IN 46634, United States
[c] Center for Advanced Radiation Sources, University of Chicago, Chicago, IL 60637, United States

ARTICLE INFO

Article history:
Received 23 February 2012
Received in revised form 2 October 2012
Accepted 20 October 2012
Available online 8 November 2012
Edited by Kei Hirose

Keywords:
Ice VII
Impurities
High-pressure H_2O
Ice planets

ABSTRACT

High-pressure H_2O polymorphs, namely ice VI, ice VII, and ice X, are hypothesized to make up a considerable portion of the interiors of large icy satellites and select extra-solar planets. The incorporation of foreign ions or molecules into these high-pressure phases is possible through ocean–ice interaction, rock–ice interaction at depth, or processes that occurred during accretion. Recent research concerning the effects charged ions have on ice VII has shown that these ions notably affect the structure of ice VII (Frank et al., 2006; Klotz et al., 2009). This study was designed to determine the effects of a molecular impurity on ice VII and compare those effects to both pure H_2O ice and ice with an ionic impurity. Ice samples were formed in this study via compression in a diamond anvil cell from either H_2O, a 1.60 mol% NaCl aqueous solution, a 1.60 mol% CH_3OH aqueous solution, or a 5.00 mol% CH_3OH aqueous solution and were compressed up to 71 GPa at room temperature. Ice formed from pure H_2O had no impurities whereas ices formed in the $NaCl–H_2O$ and $CH_3OH–H_2O$ systems contained the impurities Na^+ and Cl^- and CH_3OH, respectively. Pressure–volume relations were observed *in situ* by using synchrotron based X-ray diffraction and were used to determine the equations of state for ices formed in the H_2O, $NaCl–H_2O$ and $CH_3OH–H_2O$ systems. The data illustrate that ice VII formed from a NaCl-bearing aqueous solution exhibited a depressed volume when compared to that of H_2O-only ice VII at any given pressure, whereas ice VII formed from CH_3OH-bearing aqueous solutions showed an opposite trend, with an increase in volume relative to that of pure ice VII. The ices within planetary bodies will most likely have both ionic and molecular impurities and the trends outlined in this study can be used to improve density profiles of H_2O-rich planetary bodies.

1. Introduction

As exploration reaches farther out into the solar system and beyond, the understanding of planetary bodies that have been encountered has expanded as well. Before exploratory missions were sent to the outer reaches of the solar system, very little was known of the ice-rich bodies encountered there and many were assumed to be geologically inactive worlds (Consolmagno and Lewis, 1976; Reynolds and Cassen, 1979). The Voyager, Galileo, and Cassini-Huygens missions have greatly increased our understanding of the icy bodies within the solar system and illustrated that H_2O-rich planetary bodies can be extremely active and complex (Anderson et al., 1998; Gurnett et al., 1996; Khurana et al., 1998; McCord et al., 2001; Schubert et al., 1996; Sohl et al., 2002). Additionally, recent discoveries of extra-solar planetary bodies, such as Gliese 436b (or GJ 436b), an extra-solar planet hypothesized to have a significant proportion of solidified H_2O (Gillon et al., 2007), illustrates the importance of high-pressure H_2O-rich phases in planetary physics beyond the solar system. High-pressure experimental studies have provided much needed pressure–volume–temperature (*PVT*) equations of state (EoS) for solid phases of H_2O that may comprise the interiors of planets, such as GJ 436b (e.g., Hemley et al., 1987; Wolanin et al., 1997; Loubeyre et al., 1999; Asahara et al., 2010; Fortes et al., 2011). It is likely, however, that the high-pressure H_2O ice present within these bodies is not pure and would have trace to minor concentrations of included impurities (Frank et al., 2006, 2008). These impurities may have been incorporated into the ice structure through interactions with subsurface oceans allowing for the inclusion of either ionic or molecular impurities. Further, in a differentiated planetary body the interaction between the high-pressure H_2O phases and the surrounding silicate or metallic materials at depth may also provide a source of impurities through solid state diffusion at the elevated temperatures of planetary interiors. Therefore, a systematic study of the effects of both ionic and molecular impurities

---

* Corresponding author.
E-mail address: mfrank@niu.edu (M.R. Frank).

0031-9201/$ - see front matter © 2012 Elsevier B.V. All rights reserved.
http://dx.doi.org/10.1016/j.pepi.2012.10.010

on the structure and properties of high-pressure phases of H_2O would allow for additional constraints to be placed on the interiors of H_2O-rich planets and also provide much needed data on the incorporation of trace elements into high-pressure phases.

1.1. Impurities in high-pressure ice

Most research on the high-pressure phases of H_2O has previously been limited to the one-component H_2O system. The one-component H_2O system at high pressures is well known and has been characterized through studies using various *in situ* techniques, such as neutron and X-ray diffraction, Brillouin spectroscopy and Raman spectroscopy. Numerous experimental studies of this system have revealed that ice VI forms from liquid water at room temperature (Choukrouna and Grasset, 2007) and with increasing pressure from about 1 GPa to 2.2 GPa and has a hexagonal structure whereas ice VII is stable from 2.2 GPa to approximately 60 GPa and has a body-centered cubic structure with partially ordered hydrogen atoms (e.g., Loubeyre et al., 1999). Ice X is hypothesized to be stable at pressures greater than ~60 GPa with a structure similar to that of ice VII but ordered hydrogen throughout the lattice centered between oxygen atoms (Aoki et al., 1996; Goncharov et al., 1999; Song et al., 2003; Marx, 2006; Asahara et al., 2010). Many H_2O-rich bodies are hypothesized to have these high-pressure polymorphs of H_2O at depth, possibly in the form of mixed phases (Anderson et al., 1996, 1997; Hubbard and Marley, 1989; Khurana et al., 1998; Kuskov and Kronrod, 2005; McCord et al., 2001; Mueller and McKinnon, 1988; Nellis et al., 1988; Schubert et al., 1996; Sohl et al., 2002; Spohn and Schubert, 2003; Zimmer et al., 2000). However, there is a lack of data in geologically reasonable multi-component systems, and this can inhibit proper modeling of planetary interiors.

Only a few studies have explored the effects of impurities on ice VII. Frank et al. (2006) studied ice formed from NaCl–H_2O solutions by using X-ray diffraction and Raman spectroscopy to determine the effect that the incorporation of Na^+ and Cl^- had on the volumetric properties and crystal chemical bonding of ice VII. It was found that there was a systematic depression of the *PV* curve at 298 K relative to ice VII formed from the one-component H_2O system. This, at first glance, may seem counterintuitive as the added ions should increase the volume of the ice simply by the addition of mass. However, since NaCl dissociates into Na^+ and Cl^- ions in liquid H_2O at room temperature and ambient pressure, it was hypothesized that, upon increasing pressure, the ions would go into the open, face-centered sites of the body-centered cubic structure of ice VII. Frank et al. (2006) suggested that the charged ions in the face-centered sites attracted or repulsed the polar H_2O molecule, causing the O–H bond to rotate and become ordered within the lattice structure. This ordering of the hydrogen atoms was presumed to be similar to the ordering found in the ice X structure.

This study will examine the effect that a molecular or ionic impurity has on the lattice of the ice VII structure in an attempt to determine if the systematic depression of the unit cell volume found in the Frank et al. (2006) study was due to the charged nature of the impurity or if it was due to the presence of an impurity in the ice VII lattice, ionic or otherwise. This hypothesis was tested in this study by the compression of aqueous solutions with a molecular impurity in a diamond anvil cell to form ice VII. X-ray diffraction data taken *in situ* were used to calculate the *PVT* relations of the sample and were directly compared to the *PVT* relations of the ice VII formed in the Frank et al. (2006) study to see if there is a similar systematic variation of the unit cell volume at the same temperatures and pressures.

1.2. The ice VII-ice X phase transition

The study of the effects that may occur with the presence of impurities in high-pressure ice has mainly been limited to the high-pressure phase ice VII. This phase has a very large temperature and pressure stability field, indicating its likely relevance in the interior of large icy bodies. At pressures beyond the stability of ice VII, ice X is stable. Similar to the ice VII structure, ice X is a BCC structure, but the hydrogen–oxygen bond distance is the same between neighboring molecules with equal bonding between oxygen atoms (e.g., Aoki et al., 1996; Pruzan et al., 1997; Benoit et al., 1998; Goncharov et al., 1999; Sugimura et al., 2008). The transition from ice VII to ice X is likely complex and includes intermediate steps as a result of a double well potential (Benoit et al., 1998; Marx, 2006). It has been observed in previous studies examining the ice VII-ice X phase transition that there is a decrease in the unit cell volume of the structure (Loubeyre et al., 1999; Sugimura et al., 2008; Asahara et al., 2010). As Frank et al. (2006) found a similar decrease to the volume of the ice X structure due to the presence of an ionic impurity, the effect that impurities would have on the ice X structure, if any, merits further elucidation. This study will also compare the ice VII-ice X phase transition in pure H_2O with two different two-component systems; 1.60 mol% NaCl–H_2O and 1.60 mol% CH_3OH–H_2O to see if a transition can be observed and if impurities, either ionic or molecular, affect the transition and/or ice X structure.

2. Experimental and analytical methods

2.1. Solutions

Ice VII samples were formed from four solutions: (1) pure H_2O, (2) 1.60 mol% NaCl in H_2O, (3) 1.60 mol% CH_3OH in H_2O and (4) 5.00 mol% CH_3OH in H_2O. Aqueous solutions were prepared to examine various mole percentages of the solute, NaCl or CH_3OH, in the solvent, H_2O. The 1.60 mol% NaCl-H_2O aqueous solutions is equivalent, in mole percent, to the 5.0 wt% NaCl aqueous solution from Frank et al. (2006, 2008) and provides data on ionic impurities in ice VII and X. Frank et al. (2006) noted that ice VII forming from a NaCl–H_2O solution would incorporate Na^+ and Cl^- because, at low concentrations, the NaCl would be completely dissociated in the liquid H_2O and trapped as ionic impurities in the high pressure ice. Aqueous solutions of CH_3OH (1.60 and 5.00 mol%) were chosen because CH_3OH does not dissociate in water and therefore would exist as molecular species during the formation of ice VII. These solutions were chosen to provide a base *PV* curve (H_2O) and to provide additional *PV* data on the effects of ionic (1.60 mol% NaCl) and molecular impurities (1.60 and 5.00 mol% CH_3OH aqueous solutions) on the properties of ice VII and ice X.

2.2. Symmetric diamond anvil cell

High-pressure phases of H_2O with incorporated impurities were produced by using a symmetric diamond anvil cell (DAC). The diamond anvils were brilliant cut, had 250 μm diameter culets, and ranged from 2.26 to 2.45 mm in length from the table to the culet. Rhenium gaskets were pre-indented to approximately 30 μm and used to contain the sample between the diamonds. A 100-μm diameter hole was drilled into the indented portion of the gasket to serve as a sample chamber. Gold flakes are the pressure indicator and were added to the chamber with one of the four solutions. The gold was positioned in the chamber and then a large drop of the solution was put over the pre-indented area and quickly sealed by closing the DAC and compressing to >2 GPa to seal the chamber and form ice VII. The bubble points for the 1.6 mol% NaCl, 1.6 mol%

CH_3OH, and 5.0 mol% CH_3OH aqueous solutions are not depressed substantially below that of pure H_2O so the compositions of the solutions added during loadings were not modified by evaporation. The samples were compressed up to approximately 70, 71, 69, and 48 GPa for ices formed from H_2O, 1.60 mol% NaCl, 1.60 mol% CH_3OH, and 5.00 mol% CH_3OH aqueous solutions, respectively.

2.3. Powder X-ray diffraction

Experiments were conducted at the GSECARS 13-BM-D beam line of the Advanced Photon Source at Argonne National Laboratory. Synchrotron X-ray radiation with a monochromatic wavelength of 0.3344 Å and overall beam size of 6 × 15 μm was used for *in situ* powder diffraction analysis. The geometry of the set-up was calibrated by using CeO_2 with data processed using FIT2D software (Hammersley, 1997). The contents of the sample chamber were analyzed by using an angle dispersive powder X-ray diffraction technique with 5-min exposure times. Multiple patterns were taken over the course of 30 min to evaluate the stress of the sample. Both high-pressure ice VII (110, 200, and 211) and gold diffraction lines (111, 200, 220, and 311) were present in most of the diffraction patterns and had to be distinguished from one another, but there was little overlap between the diffraction lines of both materials throughout majority of the pressure range studied. At lower pressure, diffraction patterns of ice VII only could be obtained to index the (110) peak which overlaps with gold's (111) peak in a mixed pattern, however, the compaction of the sample chamber at higher pressures made obtaining an ice-only pattern difficult and compression was stopped once the ice (110) peak began to overlap with gold's (200) peak. Gold was used as the internal pressure indicator and its unit cell parameter (*a*) was determined at each exposure and, using the Anderson et al. (1989) EoS, a pressure was calculated. Additionally, the (200) diffraction line of Au was closely monitored to provide an indication of the stress state of the sample. The calculation of the uncertainty of the pressure determination relied on the standard deviation obtained from the mean lattice parameter calculated from the gold diffraction lines. The uncertainty of the volume of the high pressure ice was similarly determined by using all available ice diffraction lines.

3. Results

The pure H_2O, NaCl-bearing, and CH_3OH-bearing aqueous solutions were loaded into separate diamond anvil cells and pressurized to >2 GPa. The high-pressure polymorphs of H_2O and CH_3OH are transparent in the visible range and thus it is easy to observe optically any phase separation in the DAC. In general, all ice phases have different refractive indices and would exhibit relief if those two phases (or NaCl) were present in the sample chamber. Optical observations at pressures greater than 2 GPa noted only a single transparent H_2O-rich ice phase and opaque flakes of gold; no separate NaCl-rich or CH_3OH-rich phase appeared to be present in the sample chamber.

3.1. Powder X-ray diffraction

The H_2O, 1.60 and 5.00 mol% CH_3OH–H_2O, and 1.60 mol% NaCl–H_2O solutions were compressed to pressures up to 71 GPa at 298 K (Table 1). Powder diffraction data indicated that ice VII and gold were the only phases present in the sample chamber. Diffraction lines were indexed with FCC gold, Miller indices (111), (200), (220), and (311), and BCC ice VII, (110), (200), and (211) (Figs. 1–4). There were no additional peaks that suggested the presence of CH_3OH-rich or NaCl-bearing ice separates from the H_2O-rich ice, and no extra amorphous phases were observed optically in the sample chamber for experiments utilizing a methanol-bearing solution. Multiple samples were loaded and compressed to demonstrate the reproducibility of the method and to illustrate that the CH_3OH-bearing solutions did not change in composition due to preferential vaporization of methanol.

The ice VII (200) and gold (200) lines were sometimes inconsistent relative to the other diffractions lines for a given phase when a pattern was taken after a pressure increase. This suggests the sample was under some deviatoric stress (Meng et al.,1993), however, diffraction patterns collected tens of minutes after the pressure increase did not exhibit stresses beyond those related to the uncertainty in the pressure measurement. Thus, the retrieved lattice parameter and cell volumes of all ice VII samples were obtained from diffraction patterns collected after the deviatoric stress lessened and, as a result, produced a mostly smooth *PV* curve with only slight deviations from the projected trends. A noted exception to this is an apparent dip in the volumes of all ice samples occurring at approximately 50–55 GPa and becoming more pronounced at 60 GPa. The decrease in volume at these pressures flattened out a bit as the pressure was increased to 70 GPa, but no substantial and unambiguous change in volume was noticed within the precision of our experiments at the supposed transition of ice VII to ice X at approximately 60 GPa.

3.2. Isothermal compression at 298 K

The ice VII diffraction lines (110), (200), and, where present, (211) were used to calculate its unit cell parameter (*a*). The unit cell parameter was then used to calculate the volume of ice VII in Å^3. The ice VII *PV* data from the various solutions were each fit to a third-order Birch–Murnaghan EoS (Birch, 1978):

$$P(GPa) = \frac{3}{2}K_{T0}\left[\left(\frac{V_0}{V}\right)^{\frac{7}{3}} - \left(\frac{V_0}{V}\right)^{\frac{5}{3}}\right] \times \left[1 - \frac{3}{4}(4 - K'_{T0})\left(\left(\frac{V_0}{V}\right)^{\frac{2}{3}} - 1\right)\right]$$

where K_{T0}, K'_{T0}, and V_0 are, respectively, the bulk modulus, its pressure derivative, and the zero-pressure volume of ice VII. As ice VII is not a quenchable phase, the zero-pressure volume has to be either assumed or calculated along with the other two variables. The compression data for ice VII formed from H_2O are broadly consistent with previous studies and give K_{T0}, K'_{T0}, and V_0 of 20.14 ± 1.1 GPa, 4.62 ± 0.07, and 40.8 ± 0.33 Å^3, respectively (Fig. 5) with a Q-factor of 0.71. The addition of 1.60 mol% Na^+ and Cl^- to ice VII resulted in a decrease of V_0 to 38.96 ± 0.08 Å^3 with K_{T0} of 26.47 ± 0.46 GPa and K'_{T0} of 4.27 ± 0.03 and an overall Q-fit of 0.02 (Fig. 6). Ice VII samples formed from CH_3OH–H_2O solutions had an opposite trend in volume with an observed increase relative to pure H_2O at any given pressure (Fig. 7). The V_0, K_{T0}, and K'_{T0} were found to be 41.0 ± 0.19 Å^3, 21.53 ± 0.68 GPa, and 4.37 ± 0.04 for ice VII formed from a 1.60 mol% CH_3OH aqueous solution; Q was 0.965. Ice VII formed from a 5.00 mol% CH_3OH aqueous solution had an even greater increase in V_0 to 41.0 ± 0.19 Å^3 with a K_{T0} of 19.58 ± 1.08 GPa and K'_{T0} of 4.62 ± 0.04; Q was 0.01 (Fig. 8).

The most readily observable trend in the compilation of all of the ice VII data is that the addition of Na^+ and Cl^- resulted in a decrease in the volume of ice VII relative to that formed from H_2O (Fig. 9). The data from Frank et al. (2006) are consistent with the data obtained in this study, although their data has greater scatter. In contrast, the addition of CH_3OH (either 1.60 or 5.00 mol%) produced ice VII with a noticeably larger volume relative to pure H_2O systems. These opposite effects suggest the incorporation of Na^+ and Cl^- into ice VII does not produce the same structural ef-

Table 1
Pressure–volume data for ice VII collected at 295 K. The uncertainties are 2σ standard deviation from the mean.

Ice VII formed from H_2O		Ice VII formed from 1.60 mol% NaCl–H_2O		Ice VII formed from 1.60 mol% CH_3OH–H_2O		Ice VII formed from 5.00 mol% CH_3OH–H_2O	
Pressure (GPa)	Volume (Å^3)	Pressure (GPa)	Volume (Å^3)	Pressure (GPa)	Volume (Å^3)	Pressure (GPa)	Volume (Å^3)
2.30 ± 0.29	37.17 ± 0.30	6.58 ± 0.37	32.72 ± 0.05	2.56 ± 0.08	37.29 ± 0.09	3.22 ± 0.18	36.55 ± 0.02
3.89 ± 0.35	35.66 ± 0.03	7.73 ± 0.41	32.03 ± 0.03	4.57 ± 0.37	35.05 ± 0.07	5.59 ± 0.50	34.64 ± 0.04
4.35 ± 0.22	35.10 ± 0.01	9.16 ± 0.58	31.48 ± 0.10	6.54 ± 0.14	33.59 ± 0.01	5.75 ± 0.30	34.21 ± 0.02
5.03 ± 0.27	34.64 ± 0.02	9.76 ± 0.21	31.21 ± 0.04	7.56 ± 0.23	32.91 ± 0.10	6.01 ± 0.36	34.07 ± 0.01
5.79 ± 0.37	34.00 ± 0.04	11.27 ± 0.29	30.38 ± 0.01	7.73 ± 0.38	32.85 ± 0.02	7.78 ± 0.03	32.64±0.06
7.86 ± 0.17	32.49 ± 0.01	13.6 ± 0.10	29.36 ± 0.03	8.52 ± 0.41	32.40 ± 0.04	8.98 ± 0.45	32.07 ± 0.05
9.33 ± 0.39	31.82 ± 0.14	17.37 ± 0.57	28.15 ± 0.03	8.64 ± 0.52	32.30 ± 0.03	11.90 ± 0.12	30.71 ± 0.03
11.63 ± 0.23	30.30 ± 0.11	19.99 ± 0.48	27.36 ± 0.03	9.40 ± 0.26	31.85 ± 0.02	13.12 ± 0.52	30.11 ± 0.06
14.58 ± 0.12	29.25 ± 0.01	24.78 ± 0.10	26.22 ± 0.10	10.52 ± 0.13	31.28 ± 0.01	15.92 ± 0.60	29.02 ± 0.03
16.98 ± 0.37	28.44 ± 0.02	26.76 ± 0.33	25.70 ± 0.10	11.65 ± 0.49	30.85 ± 0.03	16.77 ± 0.37	28.76 ± 0.06
18.47 ± 0.63	27.97 ± 0.02	28.65 ± 0.87	25.37 ± 0.05	12.02 ± 0.49	30.49 ± 0.03	18.28 ± 0.10	28.30 ± 0.03
19.24 ± 0.06	27.70 ± 0.02	31.35 ± 0.51	24.89 ± 0.06	12.37 ± 0.43	30.37 ± 0.02	18.79 ± 0.16	27.99 ± 0.06
20.91 ± 0.54	27.26 ± 0.02	34.39 ± 0.12	24.38 ± 0.04	13.07 ± 0.34	30.14 ± 0.01	19.62 ± 0.59	27.76 ± 0.03
22.64 ± 0.51	26.83 ± 0.02	37.66 ± 0.21	23.90 ± 0.08	13.38 ± 0.10	29.94 ± 0.05	19.99 ± 0.17	27.71 ± 0.06
24.41 ± 0.88	26.38 ± 0.03	38.65 ± 0.47	23.71 ± 0.06	14.04 ± 0.48	29.71 ± 0.02	21.76 ± 0.23	27.23 ± 0.01
26.43 ± 0.57	25.96 ± 0.10	39.38 ± 0.44	23.59 ± 0.03	14.70 ± 0.31	29.49 ± 0.01	23.28 ± 0.77	26.84 ± 0.04
29.73 ± 0.34	25.34 ± 0.10	40.27 ± 0.75	23.48 ± 0.01	16.24 ± 0.16	28.92 ± 0.02	24.15 ± 0.65	26.73 ± 0.02
31.99 ± 0.76	24.89 ± 0.13	42.03 ± 0.24	23.25 ± 0.01	16.35 ± 0.16	28.86 ± 0.04	29.37 ± 0.19	25.60 ± 0.04
33.35 ± 0.71	24.77 ± 0.18	44.61 ± 0.50	22.91 ± 0.01	17.10 ± 0.67	28.59 ± 0.03	31.30 ± 0.36	25.17 ± 0.01
34.63 ± 0.72	24.53 ± 0.12	48.38 ± 0.60	22.46 ± 0.02	18.02 ± 0.07	28.38 ± 0.10	32.33 ± 0.78	24.97 ± 0.03
36.29 ± 0.45	24.07 ± 0.08	50.17 ± 0.41	22.13 ± 0.10	19.68 ± 0.20	27.99 ± 0.15	33.70 ± 0.05	24.67 ± 0.01
38.24 ± 0.64	23.95 ± 0.10	53.73 ± 0.36	21.80 ± 0.05	20.06 ± 0.24	27.67 ± 0.01	35.85 ± 0.10	24.24 ± 0.03
38.87 ± 0.65	23.83 ± 0.07	55.36 ± 0.51	21.69 ± 0.10	21.56 ± 0.22	27.44 ± 0.08	37.83 ± 0.08	24.05 ± 0.01
40.51 ± 0.89	23.57 ± 0.10	57.86 ± 0.54	21.44 ± 0.02	22.11 ± 0.48	27.15 ± 0.04	41.24 ± 0.67	23.73 ± 0.06
41.83 ± 0.57	23.38 ± 0.12	61.76 ± 0.49	21.10 ± 0.08	23.37 ± 0.23	26.83 ± 0.02	42.70 ± 0.23	23.40 ± 0.05
44.89 ± 0.62	23.03 ± 0.10	62.99 ± 0.35	20.98 ± 0.05	24.86 ± 0.21	26.38 ± 0.02	43.75 ± 0.81	23.24 ± 0.04
48.08 ± 0.38	22.70 ± 0.15	63.49 ± 0.79	20.93 ± 0.02	25.42 ± 0.23	26.29 ± 0.04	44.97 ± 0.59	23.08 ± 0.06
49.18 ± 0.97	22.47 ± 0.18	64.57 ± 0.47	20.87 ± 0.07	26.90 ± 0.35	25.94 ± 0.04	45.55 ± 0.59	22.95 ± 0.02
51.00 ± 0.91	22.25 ± 0.14	66.19 ± 0.45	20.67 ± 0.06	29.13 ± 0.21	25.55 ± 0.10	46.21 ± 0.82	22.91 ± 0.08
52.47 ± 0.81	22.14 ± 0.14	69.73 ± 0.20	20.37 ± 0.08	30.51 ± 0.51	25.26 ± 0.06	47.56 ± 0.20	22.75 ± 0.05
53.06 ± 0.85	22.07 ± 0.09	70.86 ± 0.32	20.31 ± 0.05	31.28 ± 0.32	25.08 ± 0.03		
55.24 ± 0.42	21.81 ± 0.09			33.23 ± 0.44	24.72 ± 0.05		
56.25 ± 0.60	21.70 ± 0.07			33.58 ± 0.57	24.68 ± 0.03		
59.46 ± 0.81	21.38 ± 0.08			34.28 ± 0.42	24.54 ± 0.02		
61.30 ± 0.62	21.16 ± 0.06			35.61 ± 0.53	24.31 ± 0.07		
63.70 ± 0.76	20.89 ± 0.06			41.93 ± 0.67	23.34 ± 0.08		
66.94 ± 0.68	20.74 ± 0.10			44.30 ± 0.27	23.06 ± 0.05		
68.65 ± 0.24	20.63 ± 0.05			45.30 ± 0.76	22.90 ± 0.07		
70.05 ± 0.99	20.53 ± 0.10			46.83 ± 0.79	22.72 ± 0.08		
				49.01 ± 0.61	22.47 ± 0.03		
				50.06 ± 0.73	22.33 ± 0.07		
				51.83 ± 0.30	22.14 ± 0.02		
				53.18 ± 0.61	21.99 ± 0.05		
				54.85 ± 0.87	21.85 ± 0.09		
				58.37 ± 0.05	21.52 ± 0.09		
				63.47 ± 0.48	21.03 ± 0.10		
				66.08 ± 0.46	20.80 ± 0.05		
				68.01 ± 0.97	20.69 ± 0.02		
				69.37 ± 0.87	20.55 ± 0.06		

fects as the incorporation of molecular CH_3OH. The difference in ice volumes is greatest at low pressures and decreases with increasing pressure up to approximately 45 GPa where the volumetric differences are within the uncertainty of the measurement. Finally, a decrease in all ice volumes was observed at approximately 50 GPa and again at 60 GPa relative to the EoS for ice VII formed from H_2O.

4. Discussion

4.1. Isothermal compression of H_2O ice VII

The isothermal compression data of the molecular study were compared to several pure ice VII compression studies (Fig. 10 and Table 2). The V_0 determined in this study, 40.8 ± 0.33 Å^3, is broadly consistent with all of the previous studies except that of Loubeyre et al. (1999), they reported a value of 48.2 Å^3. The K_{T0} (GPa) determined in this study for pure ice VII is approximately 15% less than those of Liu (1982), Hemley et al. (1987) and Fei et al. (1993), but is approximately 30% greater than the K_{T0} of Wolanin et al. (1997). Additionally, this study's reported K'_{T0} is 10% greater than those of Hemley et al. (1987) and Fei et al. (1993) and 25% less than Wolanin et al. (1997). A comparison of the model *PV* curves from all studies (Fig. 10) illustrates that the data from this study are at generally lower volumes for any given pressure when compared to the Hemley et al. (1987), Fei et al. (1993) and Frank et al. (2004) studies, but at greater volumes than those suggested by the EoS from Wolanin et al. (1997) and Loubeyre et al. (1999). The observed deviations in the published *PVT* models is produced by the lack of a control on the V_0, a result of the non-quenchable nature of ice VII, and the compressibility of ice VII in the 10–40 GPa range showing the greatest variability. Generally, these factors produce a group of models suggesting a less compressible ice VII, including Liu (1982), Hemley et al. (1987) and Fei et al. (1993), and a more compressible one, such as Wolanin

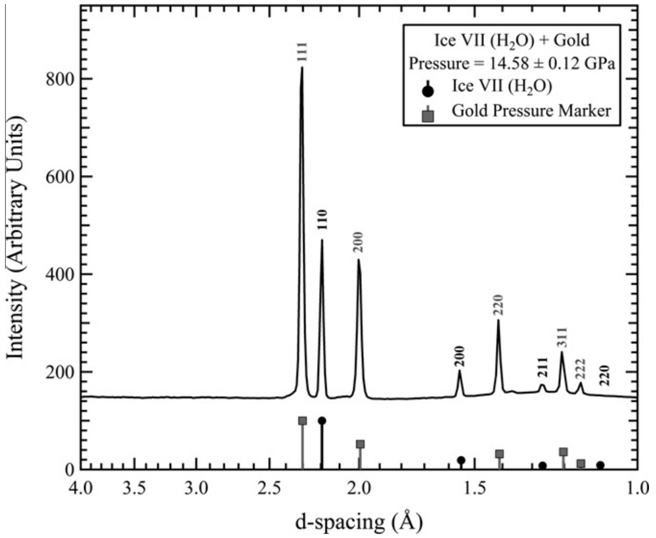

Fig. 1. Diffraction pattern of ice VII formed from H_2O. A pressure of 14.57 ± 0.12 GPa was estimated from the gold diffraction lines (1 1 1), (2 0 0), (2 2 0), (3 1 1), and (2 2 2). Ice VII diffraction lines (1 1 0), (2 0 0), and (2 1 1) were used to calculate a volume corresponding to this pressure.

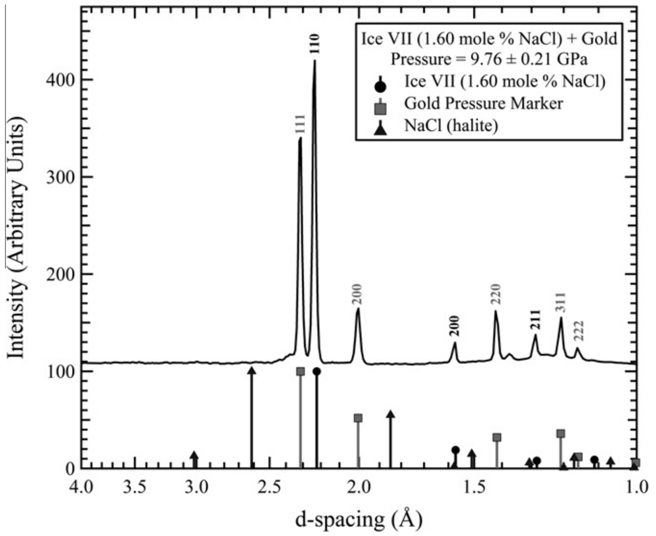

Fig. 2. Diffraction pattern of ice VII at 9.76 ± 0.21 GPa formed from a 1.60 mol% NaCl–H_2O aqueous solution. All diffractions lines can be attributed to gold, the pressure marker, or ice VII. No diffraction lines indicative of NaCl were present. Ice VII diffraction lines from (1 1 0) and (2 0 0) were detected in the experimental runs and used to determine *a* for the ice VII formed from the NaCl–H_2O aqueous solution.

et al. (1997) and Loubeyre et al. (1999), with the data from this study and Frank et al. (2004) falling in between these end members.

Recent studies have suggested that the ice VII diffraction lines may split indicating a modulated structure and suggesting a lowering of symmetry at high pressure (Somayazulu et al., 2008). However, neutron diffraction data are consistent with a cubic structure (e.g., Kuhs et al., 1984; Nelmes et al., 1993). Although we did observe minor peak splitting in some of our patterns, the splitting was spurious and not consistent and may be due to large shear stresses (Ahart et al., 2011). Furthermore, the unit cell volume calculated from the three observable ice VII diffraction lines were consistent within the established uncertainty and indicate that analyzing the diffraction patterns assuming a BCC ice VII phase is appropriate for comparing PV data and calculating K_{T0} and K'_{T0}.

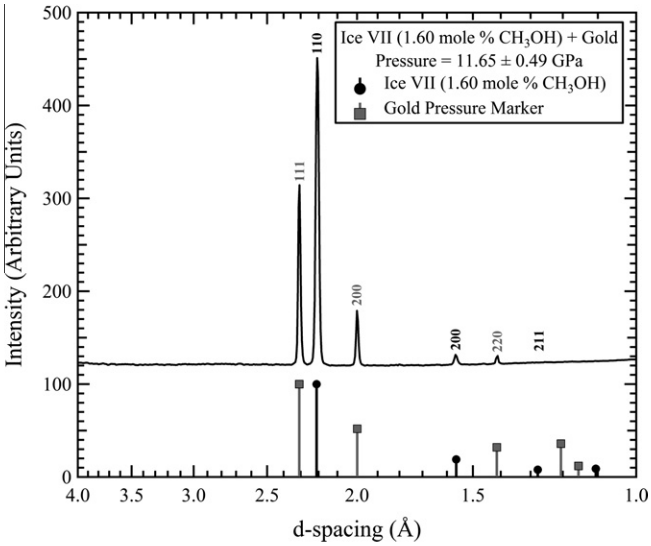

Fig. 3. Diffraction pattern of ice VII formed from a 1.60 mol% CH_3OH–H_2O aqueous solution and at 11.65 ± 0.49 GPa. The gold diffraction lines (1 1 1), (2 0 0), and (2 2 0) and the ice VII diffraction lines (1 1 0) and (2 0 0) were the only diffraction lines present in the pattern. There was no evidence of CH_3OH existing as a separate phase.

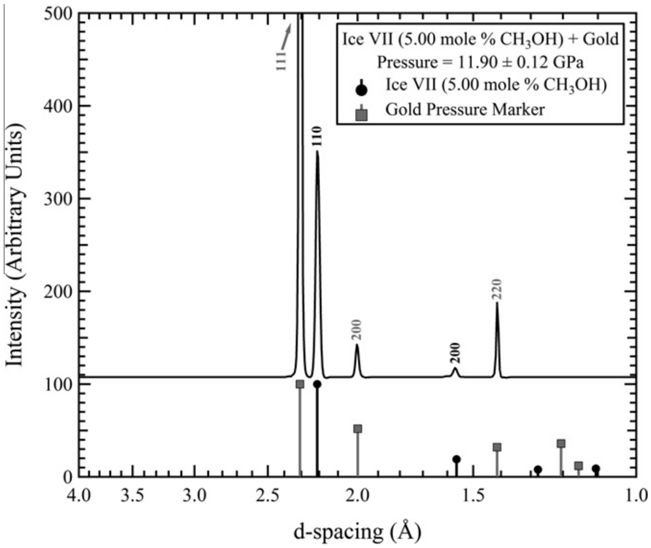

Fig. 4. Ice VII formed from a 5.00 mol% CH_3OH–H_2O aqueous solution. A pressure of 11.65 ± 0.49 GPa was estimated from the gold diffraction lines. No diffraction lines indicative of CH_3OH were noted in any X-ray diffraction pattern, suggesting that all of the CH_3OH was incorporated into the ice VII structure. Ice VII diffraction lines from (1 1 0) and (2 0 0) were used to determine *a* for the ice VII formed from the CH_3OH–H_2O aqueous solution.

4.2. Isothermal compression of ice VII formed with NaCl

Frank et al. (2006) noticed a systematic decrease in the unit cell volume of ice VII when ionic impurities, Na^+ and Cl^-, were present. Furthermore, they suggested that the incorporation of ionic impurities into the BCC structure of ice VII would result in a partial ordering of hydrogen which is akin to the ice X structure. This contention is supported by their *PV* data, which project up to a more dense structure of ice X, as well as Raman spectroscopic measurements showing a decrease in the OH^- bond length with the addition of Na^+ and Cl^-. They suggested this resulted in an ice X-like structure, where the protons are equidistant between the oxygen

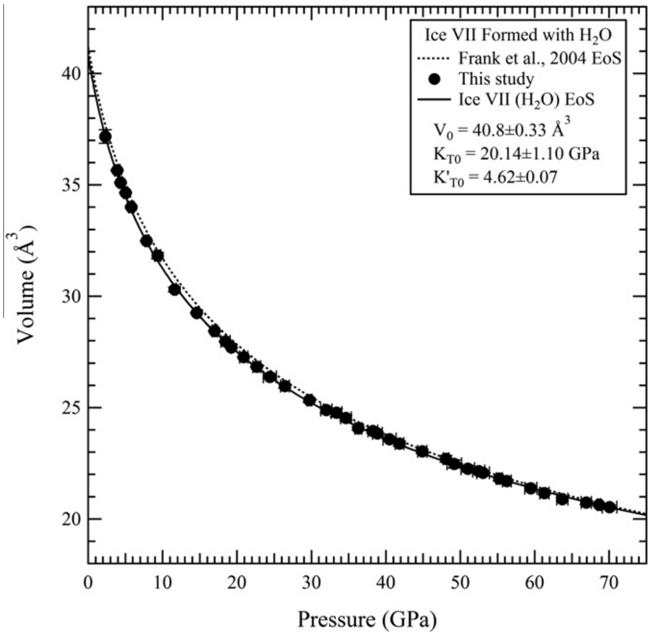

Fig. 5. X-ray diffraction data were used to calculate an isothermal equation of state at 295 K for ice VII formed from H_2O. The solid circles represent individual *PV* data whereas the error bars are calculated following the methods outlined in the text and are 2σ. A third-order Birch–Murnaghan equation of state (EoS) was fitted to the data and produced a zero-pressure volume (V_0), bulk modulus (K_{T0}), and its pressure derivative (K'_{T0}). The EoS from Frank et al. (2004) is drawn for comparison.

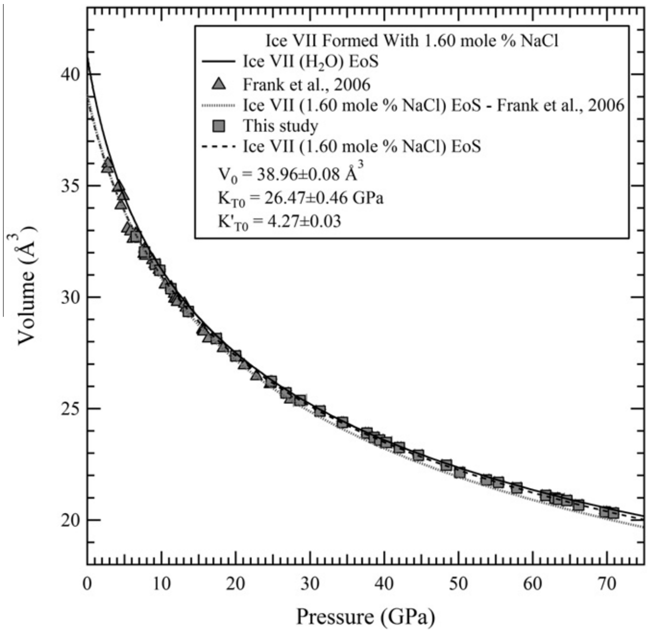

Fig. 6. Pressure-volume data for ice VII formed from a 1.60 mol% NaCl aqueous solution at 295 K. At any given pressure, the data have consistently lower volumes relative to ice VII formed from pure H_2O. Frank et al. (2006) conducted a study in the same system, but their data were limited to less than 28 GPa whereas we collected data up to approximately 70 GPa. Both data sets compare favorably and a third-order Birch–Murnaghan equation of state (EoS) was fitted to all of the *PV* data.

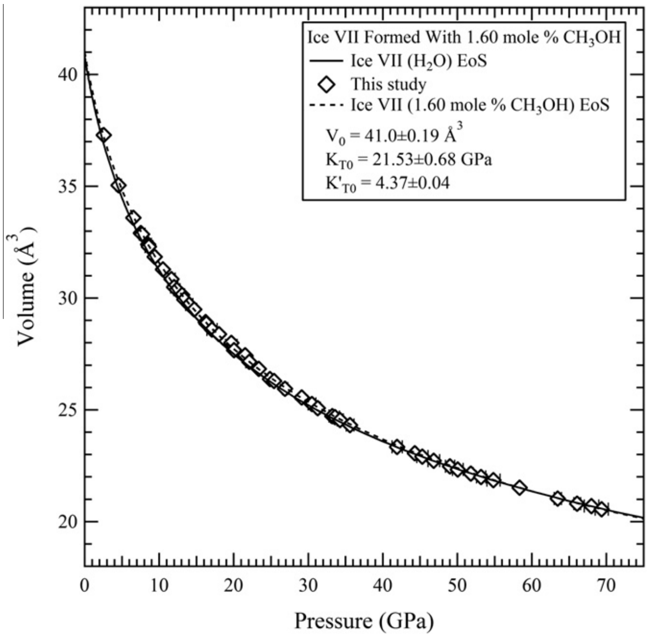

Fig. 7. The pressure–volume relations of ice VII formed from a 1.60 mol% CH_3OH aqueous solution at 295 K are compared to the EoS for pure ice VII. The data for CH_3OH-bearing ice at pressures up to 40 GPa are at systematically elevated volumes when compared to those expected for pure ice, but, at pressures great than 40 GPa, the CH_3OH-bearing ice is indistinguishable from pure ice VII.

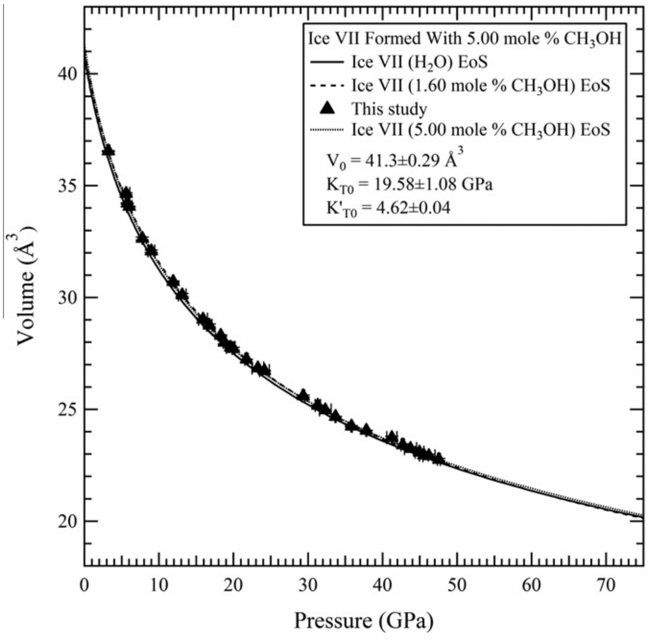

Fig. 8. X-ray diffraction data for ice VII formed from a 5.00 mol% CH_3OH aqueous solution are compared to the EoS for pure ice and ice with 1.60 mol% CH_3OH. The data show an increase in volume compared to pure ice and a slight increase relative to ice with 1.60 mol% CH_3OH.

atoms, at much lower pressures than found in pure H_2O systems. The *PV* data from this study for ice VII formed from a 1.60 mol% NaCl aqueous solution were found to be consistent with Frank et al. (2006) (Fig. 6). The data presented here extended the pressure range up to approximately 71 GPa from the previous maximum pressure of 27.34 GPa and allowed for a more precise determination of V_0, K_{T0}, and K'_{T0} (Table 2). The K_{T0} of ice VII doped with Na^+ and Cl^- was greater than that of pure ice whereas the K'_{T0} was found to decrease illustrating the Na^+ and Cl^- stiffened the ice's structure. The K_{T0} and K'_{T0} values reported by Frank et al. (2006) were 25.7 ± 0.4 and 4.15 which are consistent with the values found in this study. The data do not show a substantial change

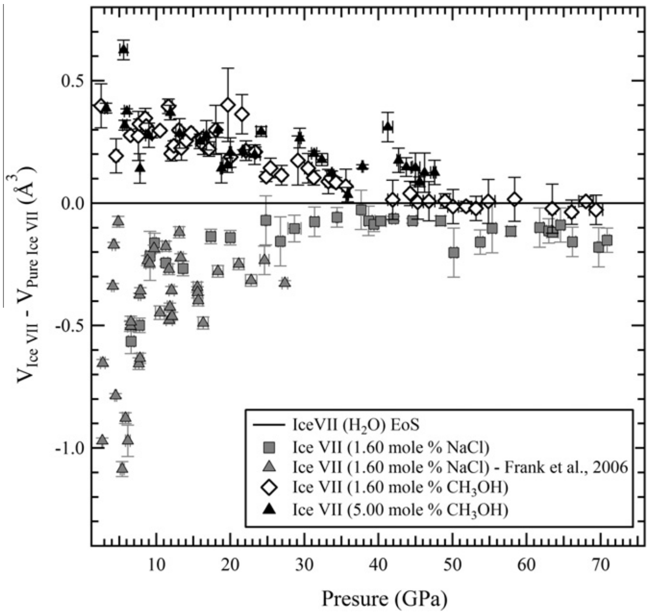

Fig. 9. The pressure–volume data for all ice VII samples with either NaCl or CH_3OH as an impurity are presented as function of pressure. The $V_{\text{Ice VII}} - V_{\text{Pure Ice VII}}$ term is the calculated difference between the measured volume and that predicted for pure ice VII at the same pressure. Ice formed from a NaCl-bearing solution was found to decrease volumetrically compared to pure ice whereas the incorporation of CH_3OH into ice VII produced an overall opposite effect and expanded the volume relative to pure ice. Samples formed with 1.60 mol% CH_3OH became indistinguishable from pure ice at pressures greater than 40 GPa while higher concentrations of CH_3OH produced a greater difference at those same pressures.

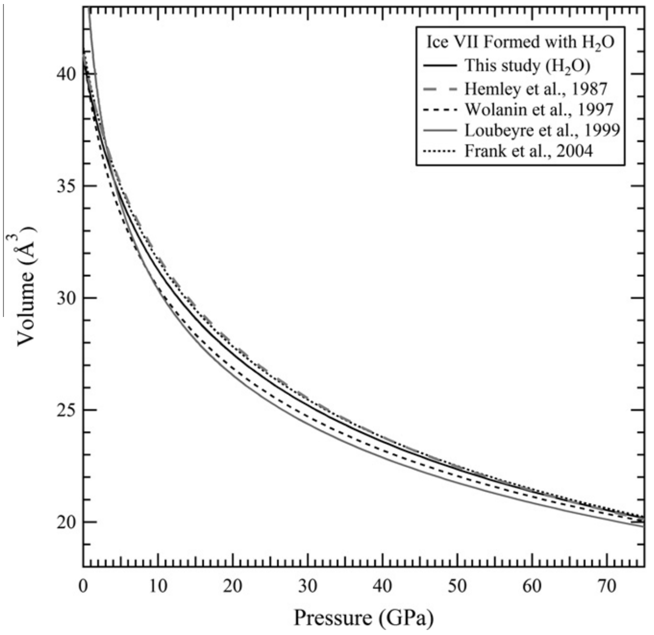

Fig. 10. A comparison of select pressure–volume equations of state (EoS) for ice VII formed from pure H_2O at room temperature. The EoS presented in this study implies a slight depressed volume relative to Hemley et al. (1987) and Frank et al. (2004), but an elevated volume relative to Wolanin et al. (1997) and Loubeyre et al. (1999). The differences in these models underline the inherent uncertainty associated with high pressures studies and are likely the result of variable pressure markers and their equations of state as well as the difficulty of working with highly compressible sample.

Table 2

This is a comparison of the zero-pressure volume V_0), bulk modulus (K_{T0}), and pressure derivative (K'_{T0}) of pure ice VII (Fei et al., 1993; Frank et al., 2004; Hemley et al., 1987; Liu, 1982; Loubeyre et al., 1999; Wolanin et al., 1997) and ice VII formed from a 1.60 mol% NaCl–H_2O aqueous solution (Frank et al., 2006) to ice VII formed from the H_2O, NaCl–H_2O, and CH_3OH–H_2O solutions of this study.

	V_0 (Å^3)	K_{T0} (GPa)	K'_{T0}
Ice VII compression EoS			
One-component, H_2O	40.8 ± 0.33	20.14 ± 1.11	4.62 ± 0.07
1.60 mol% NaCl–H_2O	38.96 ± 0.08	26.47 ± 0.46	4.27 ± 0.03
1.60 mol% CH_3OH–H_2O	41.0 ± 0.19	21.53 ± 0.68	4.37 ± 0.04
5.00 mol% CH_3OH–H_2O	41.3 ± 0.29	19.58 ± 1.08	4.62 ± 0.04
Previous ionic impurity study – 1.60 mol% NaCl–H_2O			
Frank et al. (2006)	39.1 ± 0.1	25.7 ± 0.4	4.15
Select previous one component (H_2O) studies			
Frank et al. (2004)	41.2 ± 0.1	21.3 ± 1.3	4.4 ± 0.1
Fei et al. (1993)	40.9 ± 0.7	23.9 ± 0.7	4.2 ± 0.5
Hemley et al. (1987)	40.9 ± 0.9	23.7 ± 0.9	4.15 ± 0.07
Loubeyre et al. (1999)[a]	48.2	4.26	7.75
Liu (1982)	42.2 ± 0.3	24.6 ± 0.9	4.4
Wolanin et al. (1997)[b]	41.1 ± 0.3	14.9 ± 0.8	5.4 ± 0.1
Wolanin et al. (1997)[c]	40.2 ± 0.3	14.9 ± 0.8	6.2 ± 0.1

[a] Data were obtained from a single crystal and were fit to the Vinet equation of state (Vinet et al., 1987).

[b] Data were fit to the Birch–Murnaghan equation of state (Birch, 1978).

[c] Data were fit to the Vinet equation of state (Vinet et al., 1987).

in volume at the reported ice VII-ice X phase transition pressure, but a slight decrease in volume was observed at approximately 50 and again at 62 GPa and thus, tentatively support the hypothesis of an ice X-like structure as proposed by Frank et al. (2006) and the intermediate transitional steps suggested by Benoit et al. (1998) and in the modeling of Marx (2006).

4.3. Isothermal compression of ice VII formed with CH_3OH

The isothermal compression data on ice VII formed from two CH_3OH aqueous solutions (1.60 and 5.00 mol%) data were compared to those for pure ice VII from this study, Hemley et al. (1987), Fei et al. (1993), Wolanin et al. (1997), Loubeyre et al. (1999) and Frank et al. (2004) as well as the data from NaCl-doped ice VII (Frank et al., 2006; and Figs. 7 and 8 of this study). While a systematic decrease in volume was noted in NaCl doped ice VII, the presence of CH_3OH resulted in a measureable increase in the unit cell volume for any given pressure up to 40 GPa when compared to ice VII formed from pure H_2O and when doped with Na^+ and Cl^-. At pressures greater than 40 GPa, the calculated volume of ice VII formed from the 1.60 mol% CH_3OH solution was indistinguishable from that of pure ice. The *PV* data for 5.00 mol% CH_3OH ice VII are slightly elevated relative to that of the 1.60 mol% CH_3OH data, but, unlike those data, remain elevated relative to pure ice at pressures greater than 40 GPa (Fig. 9). These data illustrate that the addition of CH_3OH produces an expanded unit cell for ice VII and that the extent of this expansion is directly related to the concentration of CH_3OH.

4.4. The ice VII to ice X transition

Previous studies of the ice VII-ice X phase transition reported a small volume decrease across the transition (e.g., the data in Hemley et al., 1987). This study tried to observe this decrease in volume with the change of phase as well as determine what, if any, effect the presence of impurities would have on this phase transition. The data at pressures near 60 GPa, the transition of ice VII to ice X, do show a slight volumetric decrease which is consistent with studies hypothesizing the existence of ice X (Aoki et al., 1996; Goncharov et al., 1999; Song et al., 2003; Asahara et al., 2010), but the data do not show a decrease in volume that can be conclusively linked to ice X and instead suggest possible intermediate stages of the transition due to a double well potential (Benoit et al., 1998; Marx, 2006; Sugimura et al., 2008). The two-component system of 1.60 mol% NaCl–H_2O was found to be consistent with the previous study of Frank et al. (2006) with no discernible volume change at approximately 60 GPa. Hence, at the suggested ice VII to X phase transition, the data do not show any readily apparent change in volume for the NaCl–H_2O system. The other two-component system, 1.60 mol% CH_3OH–H_2O, was broadly consistent with the *PV* curve of H_2O and also showed a decrease in the unit cell volume at 60 GPa. Taken together, these data cannot be used to disprove the existence of ice X and that the phase transition occurs at approximately 60 GPa, but the data do suggest that volumetric change for ice formed in the NaCl–H_2O system was less pronounced than in the H_2O and CH_3OH–H_2O systems.

4.5. Structural controls on impurities in ice VII

The BCC structure of ice VII has open, face-centered sites where interstitial impurities are most likely to reside. Depending on the impurity in the face-centered sites, there may or may not be noticeable impact on the unit cell of ice VII. Our work supports the conclusions of Frank et al. (2006) that that Na^+ and Cl^- fit into the open, face-centered sites of ice VII and, due to the charges on the ions and the polar nature of the H_2O molecule, an inter-ionic, or electrostatic, attraction between the H_2O molecule and the ionic impurity caused the hydrogen of the O–H bond in the H_2O molecule to rotate towards the Cl^- ion and away from the Na^+ ion. They suggest that this caused the hydrogen to become more ordered, giving an ice X-like structure at pressures less than ~60 GPa. The result of this change to an ice X-like structure is reflected in the decrease in the unit cell volume for ice VII formed from NaCl-bearing aqueous solutions.

The incorporation of a molecular impurity, such as CH_3OH, is also hypothesized to fit into the large voids found in the face-centered sites of the ice VII BCC structure. However, this impurity does not exist as charged ions and instead remains as an associated, electrically neutral molecule. There is a small polarity to CH_3OH due to the structure of the molecule which might have caused a slight rotation of the molecule within the lattice, but the *potential* effect of this is assumed to be small or nonexistent. From the data presented in this study, it is hypothesized that there is little to no inter-ionic attraction between the polar H_2O molecule and the CH_3OH impurity and that the main impact is an expansion of the unit cell relative to that found in pure ice VII. Thus, the high-pressure ice with the CH_3OH impurity maintains *PV* properties closely allied to pure ice VII but the unit cell became progressively larger, especially at lower pressures, when compared to pure ice VII.

With the addition of impurities into the high-pressure ice phases, there must be a limit to how much of an impurity can be present in the ice VII structure before it forms an impurity-rich phase separate of the ice within the sample chamber. Frank et al. (2006) determined that a maximum amount of 2.4 ± 0.8 mol% NaCl could be incorporated into the ice VII structure. The presence of a new impurity-rich phase was confirmed by the appearance of NaCl diffraction lines in the powder X-ray diffraction data as the NaCl could not be incorporated into the unit cell of ice VII and formed a separate phase. This study was designed to test if a similar "impurity limit" could be observed in the CH_3OH–H_2O system. The presence of a second, CH_3OH-rich phase in the sample chamber would support the hypothesis that the solution was of a concentration beyond which can be stabilized in the ice VII structure. In that case, diffraction lines consistent with CH_3OH would be detected in the analyses of the powder X-ray diffraction data. No diffraction lines indicative of CH_3OH were observed in experiments utilizing aqueous solutions of 1.60 and 5.00 mol% CH_3OH; thus, there is no diffraction-based evidence for a second CH_3OH-rich phase. However, CH_3OH at high pressure has been determined to be amorphous in select instances and would be difficult to detect with X-ray diffraction techniques (Allan et al., 1998). Thus, the sample chamber was monitored constantly for any appearance of an optically distinct phase. None of the solutions of CH_3OH–H_2O displayed any optical evidence of a separate CH_3OH-rich phase and thus it was presumed that ice VII could hold a minimum of 5.00 mol% CH_3OH as an impurity. Due to absence of any data suggesting a second phase was present, it was concluded that the CH_3OH was incorporated fully into the ice VII structure.

4.6. Planetary implications: H_2O-rich planets

Ice VI and ice VII are likely to be present in the icy satellites of the solar system (e.g., Anderson et al., 2001; Scott et al., 2002) whereas ice VII and ice X might be stable in larger H_2O-rich bodies such as the extra-solar planet Gliese 436b (Gillon et al., 2007). It is probable that the ice phases in these H_2O-rich bodies are not pure and may have various impurities incorporated into those phases. The differences in the volumes of ice VII with an ionic impurity or ice VII with a molecular impurity clearly affect the densities of high-pressure ices that exist in the interiors of icy bodies and hence would influence the internal profile of any given planet inferred from modeled density depth profiles. Difficulties in applying a general correction to impure ice VII come when dealing with the possibility of the presence of both ionic and molecular impurities in the high-pressure ice. If the ice-rich region in the interior of these bodies has both molecular and ionic impurities present, then it could be assumed that the density of this layer would be a value between the less dense ice VII with a molecular impurity and the more dense ice VII with an ionic impurity, depending, of course, on the supposed proportions of the impurities. The opposite effects imposed by these impurities means that models employing pure ice VII would be a good first order approximation. However, the presence of shallow magnetic fields below the outer ice layers of the icy satellites (e.g., Khurana et al., 1998; Zimmer et al., 2000; Kivelson et al., 2000) suggest that ionic impurities may, in fact, be the dominant impurity incorporated into high pressure ices and thus the more dense ice volume should be assumed in these instances.

5. Conclusion

Pressure–volume data were collected up to approximately 71 GPa and at room temperature for ice samples formed from four aqueous solutions. The solutions were H_2O, 1.60 mol% NaCl in H_2O, 1.60 mol% CH_3OH in H_2O, and 5.00 mol% CH_3OH in H_2O. The H_2O ice was used as a baseline so that an internally consistent analysis could be conducted on the effects of NaCl and CH_3OH incorporation into high-pressure ice VII. It was hypothesized that the incorporation of any impurity into the structure of ice VII would notably affect its unit cell volume and density. Since NaCl dissociates into Na^+ and Cl^- in H_2O and CH_3OH does not dissociate, the two chosen impurities represent the end members of ionic and molecular species that could be incorporated in high pressure ice. Ice VII was formed from each of the solutions and compressed to approximately 70 GPa for all but the 5.00 mol% CH_3OH samples, which were compressed to 48 GPa. The *PV* data show that the introduction of Na^+ and Cl^- resulted in a volumetric decrease at any given pressure when compared to pure ice VII. Conversely, the presence of CH_3OH had the opposite effect and caused an increase in the ice's unit cell volume relative to pure ice VII. Frank et al. (2006) suggested that the presence of Na^+ and Cl^- would produce an inter-ionic, or electrostatic, attraction between the H_2O molecule and the ionic impurity caused the hydrogen to rotate towards the Cl^- ion and away from the Na^+ ion. Our data support their study and also suggest that a molecular impurity, which does not exert a significant electrical pull on the hydrogen in the structure, produced an enlarged unit cell. Thus, these data indicate that charged and non-charged ions/molecules that are incorporated into the ice VII structure produce an opposite effect. With both impurity varieties present, a range of acceptable densities can be established for use in modeling the density profiles of H_2O-rich bodies with one end defined by ice VII incorporating ionic impurities and the other by ice with large molecular impurities. The density of the ice VII present in a natural system would most likely fall within the range defined by these different ices.

Acknowledgements

This research was supported by the Research and Artistry Program at Northern Illinois University (MRF). Portions of this work were performed at GeoSoilEnviroCARS (Sector 13), Advanced Photon Source (APS), Argonne National Laboratory. GeoSoilEnviroCARS is supported by the National Science Foundation – Earth Sciences (EAR-0217473), Department of Energy – Geosciences (DE-FG02-94ER14466) and the State of Illinois. Use of the APS was supported by the US Department of Energy, Basic Energy Sciences, Office of Science, under Contract No. W-31-109-Eng-38.

References

Ahart, M., Somayazulu, M., Gramsch, S.A., Boehler, R., Mao, H.-K., Hemley, R.J., 2011. Brillouin scattering of H_2O ice to megabar pressures. Journal of Chemical Physics 134, 124517.

Allan, D., Clark, S., Brugmans, M., Ackland, G., Vos, W., 1998. Structure of crystalline methanol at high pressure. Physical Review B 58 (18), 809–812.

Anderson, J.D., Lau, E.L., Sjogren, W.L., Schubert, G., Moore, W.B., 1996. Gravitational constraints on the internal structure of Ganymede. Nature 384, 541–543.

Anderson, J.D., Lau, E.L., Sjogren, W.L., Schubert, G., Moore, W.B., 1997. Gravitational evidence for an undifferentiated Callisto. Nature 387, 264–266.

Anderson, J.D., Schubert, G., Jacobson, R.A., Lau, E.L., Moore, W.B., Sjogren, W.L., 1998. Distribution of rock, metals, and ices in Callisto. Science 280, 1573–1576.

Anderson, J.D., Jacobson, R.A., McElrath, T.P., Moore, W.B., Schubert, G., Thomas, P.C., 2001. Shape, mean radius, gravity field, and interior structure of Callisto. Icarus 153 (1), 157–161.

Anderson, O.L., Isaak, D.G., Yamamoto, S., 1989. Anharmonicity and the equation of state for gold. Journal of Applied Physics 65, 1534–1543.

Aoki, K., Yamawaki, H., Sakashita, M., Fujihisa, H., 1996. Infrared absorption study of the hydrogen-bong symmetrization in ice to 110 GPa. Physical Review B 54, 15673–15677.

Asahara, Y., Hirose, K., Ohishi, Y., Hirao, N., Murakami, M., 2010. Thermoelastic properties of ice VII and its high-pressure polymorphs: implications for dynamics of cold slab subduction in the lower mantle. Earth and Planetary Science Letters 299, 474–482.

Benoit, M., Bernasconi, M., Marx, D., 1998. Tunnelling and zero-point motion in high-pressure ice. Nature 392, 258–261.

Birch, F., 1978. Finite strain isotherm and velocities for single-crystal and polycrystalline NaCl at high pressures and 300 K. Journal of Geophysical Research A 83, 1257–1268.

Choukrouna, M., Grasset, O., 2007. Thermodynamic model for water and high-pressure ices up to 2.2 GPa and down to the metastable domain. Journal of Chemical Physics 127, 124506.

Consolmagno, G.J., Lewis, J.S., 1976. The evolution of icy satellite interiors and surfaces. Icarus 34 (2), 280–293.

Fei, Y., Mao, H.K., Hemley, R.J., 1993. Thermal expansivity, bulk modulus, and melting curve of H_2O-Ice VII to 20 GPa. Journal of Chemical Physics 99, 5369–5373.

Fortes, A.D., Wood, I.G., Tucker, M.G., Marshall, W.G., 2011. The *P-V-T* equation of state of D_2O ice VI determined by neutron powder diffraction in the range $0 < P < 2.6$ GPa and $120 < T < 330$ K, and the isothermal equation of state of D_2O ice VII from 2 to 7 GPa at room temperature. Journal of Applied Crystallography 45, 523–534.

Frank, M.R., Fei, Y., Hu, J., 2004. Constraining the equation of state of the fluid H_2O to 80 GPa using the melting curve, bulk modulus and thermal expansivity of Ice VII. Geochimica et Cosmochimica Acta 68 (13), 2781–2790.

Frank, M.R., Runge, C.E., Scott, H.P., Maglio, S.J., Olson, J., Prakapenka, V.B., Shen, G., 2006. Experimental study of the NaCl–H_2O system up to 28 GPa: implications for ice-rich planetary bodies. Physics of the Earth and Planetary Interiors 155, 152–162.

Frank, M.R., Scott, H.P., Maglio, S.J., Prakapenka, V.B., Shen, G., 2008. Temperature induced immiscibility on the NaCl–H_2O system at high pressure. Physics of the Earth and Planetary Interiors 170, 107–114.

Gillon, M., Pont, F., Demory, B.-O., Mallmann, F., Mayor, M., Mazeh, T., Queloz, D., Shporer, A., Udry, S., Vuissoz, C., 2007. Detection of transits of the nearby hot Neptune GJ 436 b. Astronomy and Astrophysics 472, L13–L16.

Goncharov, A.F., Struzhkin, V.V., Mao, H.K., Hemley, R.J., 1999. Raman spectroscopy of dense H_2O and the transition to symmetric hydrogen bonds. Physical Review Letters 83, 1998–2001.

Gurnett, D.A., Kurth, W.S., Roux, A., Bolton, S.J., Kennel, C.F., 1996. Evidence for a magnetosphere at Ganymede from plasma-wave observations by the Galileo spacecraft. Nature 384, 535–537.

Hammersley, A.P., 1997. FIT2D: An introduction and overview. ESRF Internal Report ESRF97HA02T.

Hemley, R.J., Jephcoat, A.P., Mao, H.K., Zha, C.S., Finger, L.W., Cox, D.E., 1987. Static compression of H_2O-Ice to 128 GPa (1.28 Mbar). Nature 330, 737–740.

Hubbard, W.B., Marley, M.S., 1989. Optimized Jupiter, Saturn, and Uranus interior models. Icarus 78, 102–118.

Khurana, K.K., Kivelson, M.G., Stevenson, D.J., Schubert, G., Russell, C.T., Walker, R.J., Polansky, C., 1998. Induced magnetic fields as evidence for subsurface oceans in Europa and Callisto. Nature 395, 777–780.

Kivelson, M.G., Khurana, K.K., Russell, C.T., Volwerk, M., Walker, R.J., Zimmer, C., 2000. Galileo magnetometer measurements: a stronger case for a subsurface ocean at Europa. Science 289, 1340–1343.

Klotz, S., Bove, L., Strassle, T., Hansen, T., Saitta, A., 2009. The preparation and structure of salty ice VII under pressure. Nature Materials 8, 405–409.

Kuhs, W.F., Finney, J.L., Vettier, C., Bliss, D.V., 1984. Structure and hydrogen ordering in ices VI, VII, and VIII by neutron powder diffraction. Journal of Chemical Physics 81, 3612.

Kuskov, O.L., Kronrod, V.A., 2005. Models of the internal structure of Callisto. Solar System Research 39 (4), 283–301.

Liu, L.-G., 1982. Compression of ice VII to 500 kbar. Earth and Planetary Science Letters 61 (2), 359–364.

Loubeyre, P., LeToullec, R., Wolanin, E., Hanfland, M., Häusermann, D., 1999. Modulated phases and proton centering in ice observed by X-ray diffraction up to 170 GPa. Nature 397, 503–506.

Marx, D., 2006. Proton transfer 200 Years after von Grotthuss: insights fromAb initio simulations. ChemPhysChem 7, 1848–1870.

McCord, T.B., Hansen, G.B., Hibbitts, C.A., 2001. Hydrated salt minerals on Ganymede's surface. Evidence of an ocean below. Science 292, 1523–1525.

Mueller, S., McKinnon, W.B., 1988. Three-layered models of Ganymede and Callisto: compositions, structures, and aspects of evolution. Icarus 76, 437–464.

Meng, Y., Weidner, D.J., Fei, Y., 1993. Deviatoric stress in a quasihydrostatic diamond anvil cell: effect on the volume-based pressure calibration. Geophysical Research Letters 20, 1147–1150.

Nellis, W.J., Hamilton, D.C., Holmes, N.C., Radousky, H.B., Rhee, F.H., Mitchell, A.C., Nicol, M., 1988. The nature of the interior of Uranus based on studies of planetary ices at high dynamic pressure. Science 240, 779–781.

Nelmes, R.J., Loveday, J.S., Wilson, R.M., Besson, J.M., Pruzan, P., Klotz, S., Hamel, G., Hull, S., 1993. Neutron diffraction study of the structure of deuterated ice VIII to l0 GPa. Physical Review Letters 71, 1192.

Pruzan, P., Wolanin, E., Gauthier, M., Chervin, J.C., Canny, B., 1997. Raman scattering and X-ray diffraction of ice in the megabar range occurrence of a symmetric disordered solid above 62 GPa. Journal of Physical Chemistry B 101 (32), 6230–6233.

Reynolds, R.T., Cassen, P.M., 1979. On the internal structure of the major satellites of the outer planets. Geophysical Research Letters 6, 121–124.

Schubert, G., Zhang, K., Kivelson, M.G., Anderson, J.D., 1996. The magnetic field and internal structure of Ganymede. Nature 384 (6609), 544–545.

Scott, H.P., Williams, Q., Ryerson, F.J., 2002. Experimental constraints on the chemical evolution of icy satellites. Earth and Planetary Science Letters 203, 399–412.

Sugimura, E., Iitaka, T., Hirose, K., Kawamura, K., Sata, N., Ohishi, Y., 2008. Compression of H_2O ice to 126 GPa and implications for hydrogen-bond symmetrization: synchrotron X-ray diffraction measurements and density-functional calculations. Physical Review B 77, 214103.

Sohl, F., Spohn, T., Breuer, D., Nagel, K., 2002. Implications from Galileo observations on the interior structure and chemistry of the Galilean satellites. Icarus 161, 104–119.

Somayazulu, M., Shu, J., Chang-sheng, Z., Goncharov, A.F., 2008. *In situ* high-pressure X-ray diffraction study of H_2O ice VII. Journal of Chemical Physics 128, 064510.

Song, M., Yamawaki, H., Fujihisa, M., Sakashita, M., Aoki, K., 2003. Infrared investigation on ice VIII and the phase diagram of dense ices. Physical Review B 68, 014106.

Spohn, T., Schubert, G., 2003. Oceans in the icy Galilean satellites of Jupiter? Icarus 161, 456–467.

Vinet, P., Smith, J.R., Ferrante, J., Rose, J.H., 1987. Temperature effect on the universal equation of state of solids. Physical Review B 35, 1945–1953.

Wolanin, E., Pruzan, P., Chervin, J.C., Canny, B., Gauthier, M., Häusermann, D., Hanfland, M., 1997. Equation of state of ice VII up to 106 GPa. Physical Review B 56, 5781–5785.

Zimmer, C., Khurana, K.K., Kivelson, M.G., 2000. Subsurface oceans on Europa and Callisto: constraints from Galileo magnetometer observations. Icarus 147, 329–347.